

Article

A SVM-3D Based Encoderless Control of a Fault-Tolerant PMSM Drive

Kamel Saleh ^{1,*} and Mark Sumner ² 

¹ Electrical Engineering Department, Faculty of Engineering and Information Technology, New Campus, An-Najah National University, Nablus P.O. Box 7, Palestine

² Electrical and Electronic Engineering Department, Faculty of Engineering, University Park, University of Nottingham, Nottingham NG7 2RD, UK; mark.sumner@nottingham.ac.uk

* Correspondence: kamel.saleh@najah.edu

Received: 28 May 2020; Accepted: 28 June 2020; Published: 4 July 2020



Abstract: This paper exhibits a novel technique to obtain an encoderless speed control of a permanent magnet synchronous motor (PMSM) in the case of a loss of one phase. The importance of this work is that it presents solutions in order to maintain the operation of the system in various conditions. This will increase the reliability of the whole drive system to meet the safety issues required in some applications. To achieve that, a fault-tolerant inverter modulated through a 3-dimension space vector pulse width modulation technique (3D-SVPWM) is used. Besides that, an algorithm to obtain the exact position of the saturation saliency in the case of a loss of one phase is introduced to achieve a closed-loop field-oriented encoderless speed control and to further enhance the reliability of the whole drive system. This algorithm is based on measuring the transient stator current responses of the motor due to the insulated-gate bipolar transistors (IGBTs) switching actions. Then according to the operating condition (normal or a loss of one phase), the saliency position signals are constructed from the dynamic current responses. Simulation results are provided to demonstrate the effectiveness of the saliency tracking technique under normal and under a loss of one phase conditions. Moreover, the results verify the maximum reliability for the whole drive system that is achieved in this work through a continuous operation of the drive system under a loss of one phase condition and under encoderless speed control.

Keywords: fault-tolerant inverter; encoderless; SVM 3D

1. Introduction

Nowadays, permanent magnet synchronous motors (PMSMs) are increasingly being used in industrial and domestic drive applications. Compared to induction motors, a PMSM has higher efficiency, higher power density, and wider speed range operation [1,2]. However, a closed-loop field-oriented control of the PMSMs cannot be achieved without precise knowledge of the rotor position. Rotor position used to be obtained using optical encoders or resolvers. However, attaching such sensors is usually associated with increasing the noise interference and reducing the reliability for the whole drive system. Therefore, there is a motivation to obtain a “sensorless” or “encoderless” closed-loop field-oriented control of the PMSM drive without using encoders or resolvers.

There are different techniques presented in the literature for a “sensorless” or “encoderless” closed-loop field-oriented control of the PMSM motors and they are divided into two main groups. The first group is known as model-based methods [3–5]. The rotor speed in these techniques is obtained by measuring the back-electro force (EMF) of the motor. These techniques are good at medium and high speeds while their performance at low speed will be low. This is related to the fact that the back EMF will vanish at low and zero speeds. Moreover, model-based methods are sensitive to

motor parameter variation. The second group is called “saliency and signal injection methods” [6–12]. Saliency and signal injection techniques do not require back-EMF information. Instead, they depend on tracking the saliency in the motor resulting from the irregular distribution of the magnetic field in the motor. These saliencies will be reflected in the inductances of the motor. Hence, by applying a kind of excitation signal (currents or voltages) and measuring the stator current’s effect due to the injected signals, the saliency position and rotor position can be obtained. These techniques give a good performance at zero and low speed under different load conditions. However, these encoderless techniques produce high audible noise, extra losses, current harmonics, torque ripples, transient disturbances, and vibration.

In certain applications like electric vehicles, aerospace systems, military, and hospitals, the shutdown of the electrical systems due to any fault in the inverter may result in a potential risk to human beings and immeasurable economic losses [13–15]. Hence, these applications require a reliable inverter that enables the continuous operation of the system in the case of a loss of one phase. Therefore, discussion of fault-tolerant inverters and enhanced system reliability attracts much attention from researchers. Fault-tolerant inverters are reported in many papers in literature. These fault-tolerant inverters make use of hardware redundancy to achieve post-fault operation [16]. Based on the hardware redundancy, the fault-tolerant inverters can be classified into three groups. The first group deals with switch faults to achieve post-fault operation using different techniques like inherently redundant switching states [17], DC-bus midpoint connection [18], and redundant parallel or series switches installation [19]. The second group deals with leg fault to achieve post-fault operation by adding redundant legs connected in parallel or series to the main legs [20,21]. Finally, post fault operation can be achieved in a multi-level inverter using three scenarios including neutral-shift, DC-bus voltage reconfiguration, and redundant modules installations [22–24].

Encoderless control of motor drives in the case of the loss of one phase is proposed in [25] using a four-leg two-level (PMSM) drive. A special fault-tolerant control technique was used in the case of a loss of one phase to keep the performance of the drive from degradation.

The importance of this work is that it presents solutions in order to maintain the operation of the system in various conditions. This can be achieved by using a 4-leg inverter which is modulated using the 3-dimension space vector pulse width modulation (3D-SVPWM) technique. In addition to using a new algorithm to track the saturation saliency in the PMSM under a single-phase open-circuit fault, this issue is quite important in some applications like vehicle and aerospace applications to increase the safety procedures and reliability for the whole system.

2. Research Method

2.1. Fault-Tolerant Drive Topology

Figure 1 introduces the fault-tolerant drive topology. An overview of each part of this topology is illustrated below.

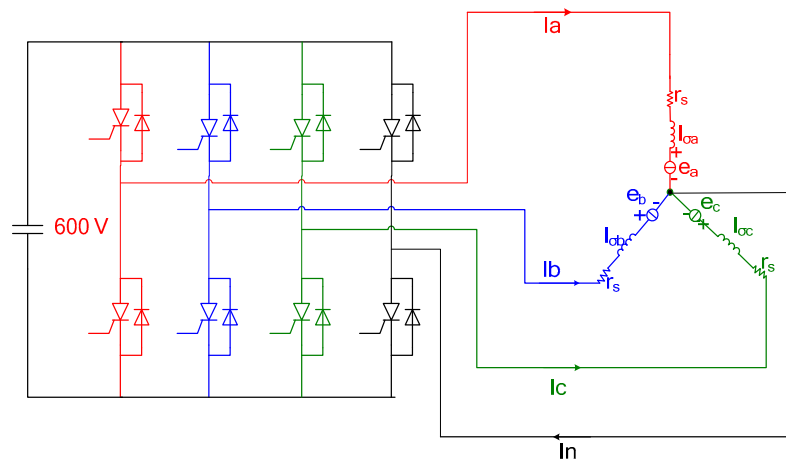


Figure 1. Four-leg permanent magnet synchronous motors (PMSM) drive.

2.1.1. Three-Phase PMSM Model

The three-phase PMSM model is given in Equations (1)–(5). In this model, the saturation saliency is inherited in the self and leakage inductances equations. Moreover, this model can give trusted results in healthy operating conditions and in the cases of some fault conditions like a single-phase open-circuit fault.

$$\begin{bmatrix} v_{an} \\ v_{bn} \\ v_{cn} \end{bmatrix} = r_s * \begin{bmatrix} i_a \\ i_b \\ i_c \end{bmatrix} + \begin{bmatrix} d\phi_a/dt \\ d\phi_b/dt \\ d\phi_c/dt \end{bmatrix} \tag{1}$$

$$\begin{bmatrix} \phi_a \\ \phi_b \\ \phi_c \end{bmatrix} = \begin{bmatrix} L_{aa} & L_{ab} & L_{ac} \\ L_{ab} & L_{bb} & L_{bc} \\ L_{ac} & L_{bc} & L_{cc} \end{bmatrix} \begin{bmatrix} i_a \\ i_b \\ i_c \end{bmatrix} + \begin{bmatrix} \phi_{ma} \\ \phi_{mb} \\ \phi_{mc} \end{bmatrix} \tag{2}$$

where $v_{an,bn,cn}$ are the stator phase voltages of the motor; r_s is the stator winding resistance; $i_{a,b,c}$ is the stator phase current; $\phi_{a,b,c}$ are the total magnetic fluxes linking each stator winding; L_{aa}, L_{bb} and L_{cc} are the stator winding’s self-inductances and L_{ab}, L_{ac} and L_{bc} are the stator winding’s mutual-inductances. $\phi_{ma,b,c}$ are magnetic fluxes linking the stator winding generated by the permanent magnet.

The stator windings’ inductances are defined by

$$\begin{bmatrix} L_{aa} \\ L_{bb} \\ L_{cc} \end{bmatrix} = \begin{bmatrix} L_{s0} + L_{sl} \\ L_{s0} + L_{sl} \\ L_{s0} + L_{sl} \end{bmatrix} + L_x * \begin{bmatrix} \cos(2\theta) \\ \cos(2\theta - 120) \\ \cos(2\theta - 240) \end{bmatrix} \tag{3}$$

$$\begin{bmatrix} L_{ab} \\ L_{ac} \\ L_{bc} \end{bmatrix} = L_{s0} * \begin{bmatrix} \cos(120) \\ \cos(240) \\ \cos(120) \end{bmatrix} + L_x * \begin{bmatrix} \cos(2\theta - 120) \\ \cos(2\theta - 120) \\ \cos(2\theta - 120) \end{bmatrix} \tag{4}$$

where L_{sl} is the stator winding’s self-inductance per phase. L_x is the stator winding’s inductance fluctuation. L_{s0} is the stator winding’s mutual inductance. The effects of saturation saliency appearing in stator self and mutual inductances are indicated by the term (2θ) .

The flux-linkages at the stator windings due to the permanent magnet are

$$\begin{bmatrix} \phi_{ma} \\ \phi_{mb} \\ \phi_{mc} \end{bmatrix} = y_m * \begin{bmatrix} \cos(\theta) \\ \cos(\theta - 120) \\ \cos(\theta - 240) \end{bmatrix} \tag{5}$$

where y_m is the peak magnetic flux linkage due to a permanent magnet.

2.1.2. Four-Leg Inverter

Figure 1 shows the proposed fault-tolerant drive configuration. In this configuration, an extra leg is introduced to the conventional inverter which is connected permanently to the motor neutral point. By using a 3D-SVPWM technique, the switches in the extra leg will be permanently activated; hence the phase to the neutral voltage that can be generated between any phase and neutral could be 600 V, zero, and -600 V.

2.1.3. 3D- Space Vector Pulse Width Modulation (3D-SVPWM)

The proposed 3D-SVPWM method that is used in this work is presented in [26]. This technique is very simple and based on geometrical consideration. More importantly, it can be used under healthy conditions and post an open circuit fault without modifications. The 3D space vector of the four-leg inverter is shown in Figure 2 in $\alpha\beta\gamma$ plane and the projection of the sixteen vectors into $\alpha\beta$ plane.

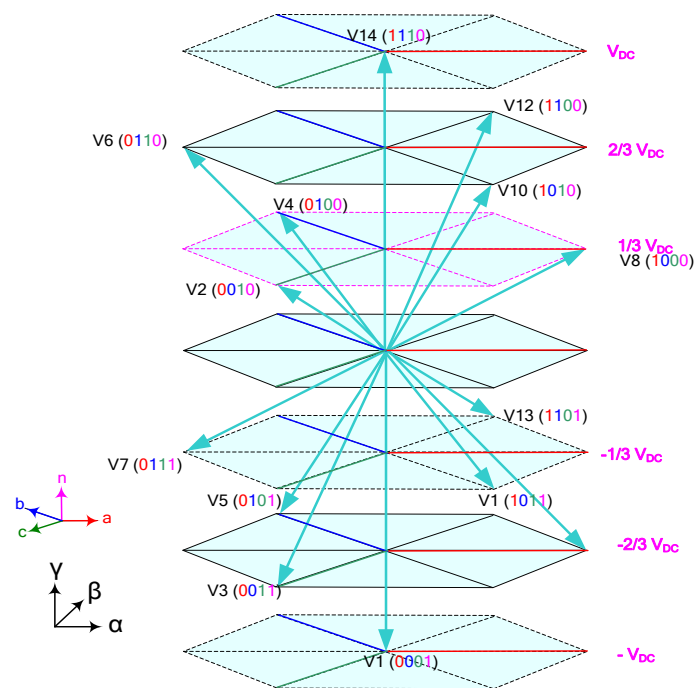


Figure 2. Three-dimension space vector pulse width modulation (3D-SVPWM) for a four-leg inverter.

The algorithm to implement the 3D-SVPWM is shown in Figure 3. A fast preview of the working of each block will be presented here.

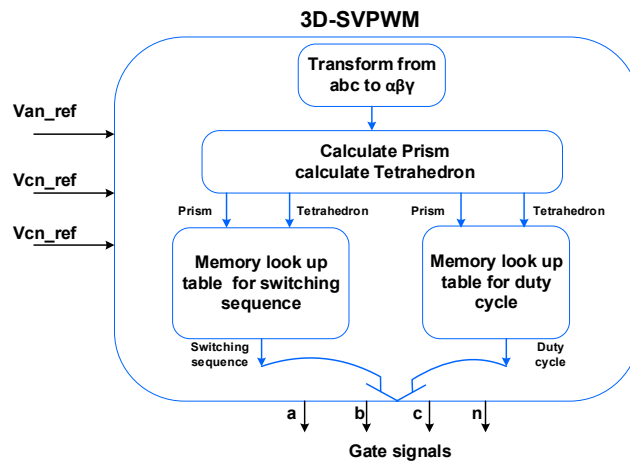


Figure 3. The algorithm of the 3D-SPVPWM.

The reference voltage (V_{ref}) can be located in any of the six prisms shown in Figure 4a. The prism can be identified by projecting the reference voltage into the $\alpha\beta$ plane shown in Figure 4b.

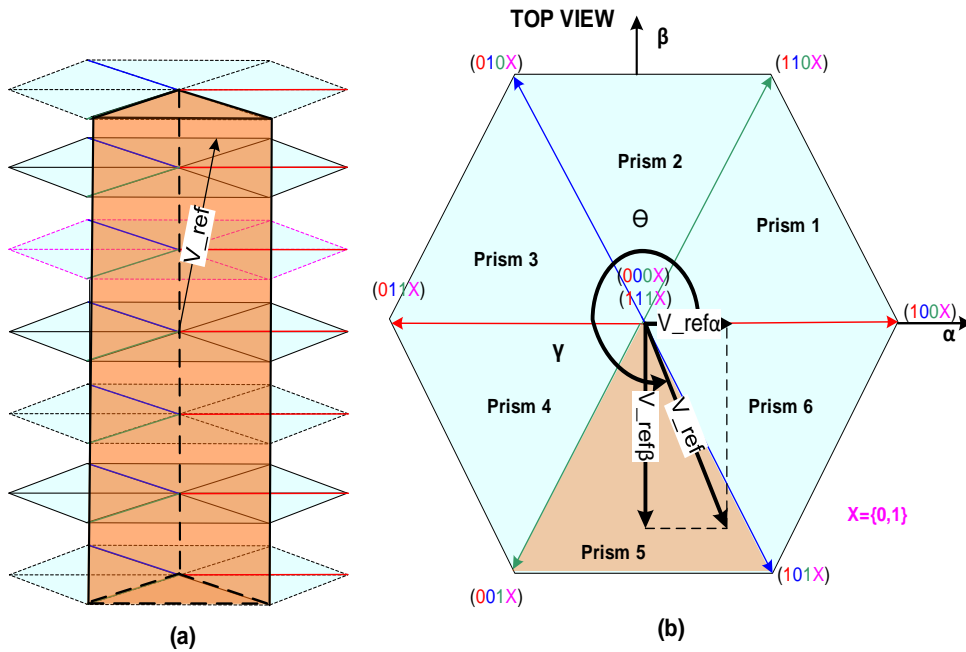


Figure 4. Switching Space Vectors in α - β - γ frame: (a) 3D-View (b) Top View.

Then the angle of the reference voltage can be calculated according to Equation (6). After the angle of the reference voltage (V_{ref}) is obtained in the $\alpha\beta$ plane then the prism can be identified according to Table 1.

$$\theta = \arctan\left(\frac{V_{ref\beta}}{V_{ref\alpha}}\right) \tag{6}$$

Table 1. Selection of the prism.

Angle of Reference Voltage (θ)	Prism Number
$0 \leq \theta < \pi/3$	1
$\pi/3 \leq \theta < 2 * \pi/3$	2
$2 * \pi/3 \leq \theta < \pi$	3
$\pi \leq \theta < 4 * \pi/3$	4
$4 * \pi/3 \leq \theta < 5 * \pi/3$	5
$5 * \pi/3 \leq \theta < 2\pi$	6

Each prism can be divided into four tetrahedrons as shown in Figure 5. The tetrahedron number can be identified using the sign of the three voltages to neutral voltages (V_{an} , V_{bn} , and V_{cn}) according to Table 2.

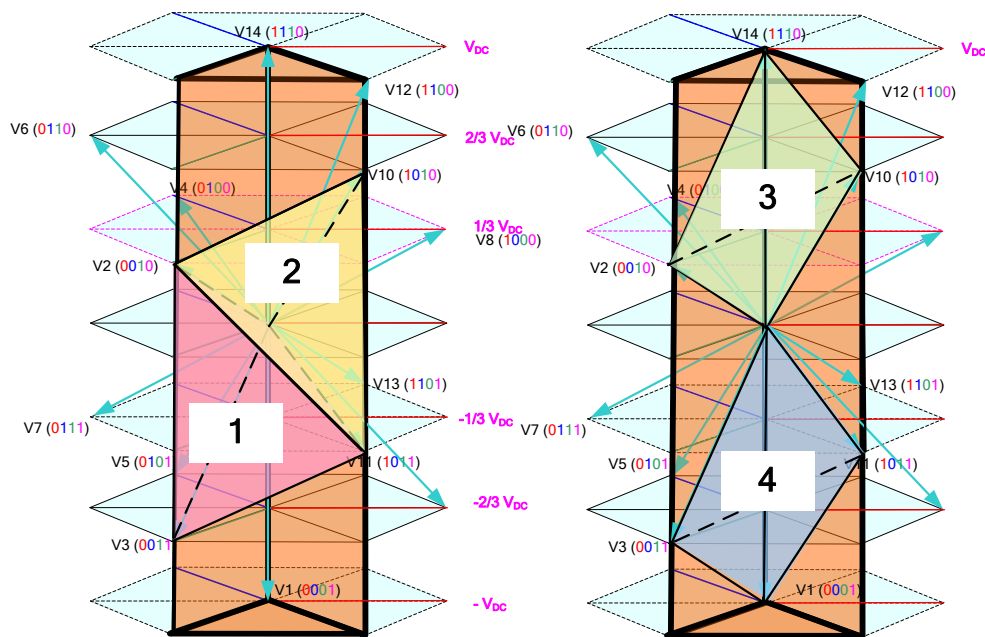


Figure 5. Tetrahedron selection.

Table 2. Selection of the tetrahedron.

Conditions			Tetrahedron
$V_{an} \geq 0$	$V_{bn} < 0$	$V_{cn} < 0$	1
$V_{an} \geq 0$	$V_{bn} \geq 0$	$V_{cn} < 0$	2
$V_{an} \geq 0$	$V_{bn} \geq 0$	$V_{cn} \geq 0$	3
$V_{an} < 0$	$V_{bn} < 0$	$V_{cn} < 0$	4

Then, after identifying the prism and the tetrahedron where the reference voltage is located, three adjacent switching active vectors in addition to the zero switching vectors (0000,1111) are chosen according to Table 3 to obtain the correct switching sequence. The time of application of the three active vectors and two zero vectors are given in Table 4.

Table 3. Look up table for choosing correct switching sequence.

Prism	Tetrahedron	Switching Active Vectors
1	1	V8,V9,V13
	2	V8,V12,V13
	3	V8,V12,V14
	4	V1,V9,V13
2	1	V4,V5,V13
	2	V4,V12,V13
	3	V4,V12,V14
	4	V1,V4,V13
3	1	V4,V5,V7
	2	V4,V6,V7
	3	V4,V6,V14
	4	V1,V5,V7
4	1	V2,V3,V7
	2	V2,V6,V7
	3	V2,V6,V14
	4	V1,V3,V7
5	1	V2,V3,V11
	2	V2,V10,V11
	3	V2,V10,V14
	4	V1,V3,V11
6	1	V8,V9,V11
	2	V8,V10,V11
	3	V8,V10,V14
	4	V1,V9,V11

Table 4. Look up table for duty cycle computation.

Prism	Tetrahedron 1	Tetrahedron 2	Tetrahedron 3	Tetrahedron 3
1	$\begin{bmatrix} 1 & 0 & 1 \\ \frac{1}{2} & \frac{-\sqrt{3}}{2} & -1 \\ 0 & \sqrt{3} & 0 \end{bmatrix}$	$\begin{bmatrix} \frac{3}{2} & \frac{-\sqrt{3}}{2} & 0 \\ -\frac{1}{2} & \frac{\sqrt{3}}{2} & 1 \\ \frac{1}{2} & \frac{\sqrt{3}}{2} & -1 \end{bmatrix}$	$\begin{bmatrix} \frac{3}{2} & \frac{-\sqrt{3}}{2} & 0 \\ 0 & \sqrt{3} & 0 \\ -\frac{1}{2} & \frac{-\sqrt{3}}{2} & 1 \end{bmatrix}$	$\begin{bmatrix} -1 & 0 & -1 \\ \frac{3}{2} & \frac{-\sqrt{3}}{2} & 0 \\ 0 & \sqrt{3} & 0 \end{bmatrix}$
2	$\begin{bmatrix} -\frac{1}{2} & \frac{\sqrt{3}}{2} & 1 \\ -1 & 0 & -1 \\ \frac{3}{2} & \frac{\sqrt{3}}{2} & 0 \end{bmatrix}$	$\begin{bmatrix} -\frac{3}{2} & \frac{\sqrt{3}}{2} & 0 \\ 1 & 0 & 1 \\ \frac{1}{2} & \frac{\sqrt{3}}{2} & -1 \end{bmatrix}$	$\begin{bmatrix} -\frac{3}{2} & \frac{\sqrt{3}}{2} & 0 \\ \frac{3}{2} & \frac{\sqrt{3}}{2} & 0 \\ -\frac{1}{2} & \frac{-\sqrt{3}}{2} & 1 \end{bmatrix}$	$\begin{bmatrix} -1 & 0 & -1 \\ -\frac{3}{2} & \frac{\sqrt{3}}{2} & 0 \\ \frac{3}{2} & \frac{\sqrt{3}}{2} & 0 \end{bmatrix}$
3	$\begin{bmatrix} -\frac{1}{2} & \frac{\sqrt{3}}{2} & 1 \\ \frac{1}{2} & \frac{\sqrt{3}}{2} & -1 \\ \frac{3}{2} & \frac{-\sqrt{3}}{2} & 0 \end{bmatrix}$	$\begin{bmatrix} 0 & \sqrt{3} & 0 \\ -\frac{1}{2} & \frac{-\sqrt{3}}{2} & 1 \\ -1 & 0 & -1 \end{bmatrix}$	$\begin{bmatrix} 0 & \sqrt{3} & 0 \\ -\frac{3}{2} & \frac{-\sqrt{3}}{2} & 0 \\ 1 & 0 & 1 \end{bmatrix}$	$\begin{bmatrix} \frac{1}{2} & \frac{-\sqrt{3}}{2} & -1 \\ 0 & \sqrt{3} & 0 \\ -\frac{3}{2} & \frac{-\sqrt{3}}{2} & 0 \end{bmatrix}$
4	$\begin{bmatrix} -\frac{1}{2} & \frac{\sqrt{3}}{2} & 1 \\ \frac{1}{2} & \frac{-\sqrt{3}}{2} & -1 \\ -\frac{3}{2} & \frac{\sqrt{3}}{2} & 0 \end{bmatrix}$	$\begin{bmatrix} 0 & -\sqrt{3} & 0 \\ -\frac{1}{2} & \frac{\sqrt{3}}{2} & 1 \\ -1 & 0 & -1 \end{bmatrix}$	$\begin{bmatrix} 0 & -\sqrt{3} & 0 \\ -\frac{3}{2} & \frac{\sqrt{3}}{2} & 0 \\ 1 & 0 & 1 \end{bmatrix}$	$\begin{bmatrix} \frac{1}{2} & \frac{\sqrt{3}}{2} & -1 \\ 0 & -\sqrt{3} & 0 \\ -\frac{3}{2} & \frac{\sqrt{3}}{2} & 0 \end{bmatrix}$
5	$\begin{bmatrix} -\frac{1}{2} & \frac{-\sqrt{3}}{2} & 1 \\ -1 & 0 & -1 \\ \frac{3}{2} & \frac{-\sqrt{3}}{2} & 0 \end{bmatrix}$	$\begin{bmatrix} -\frac{3}{2} & \frac{-\sqrt{3}}{2} & 0 \\ 1 & 0 & 1 \\ \frac{1}{2} & \frac{-\sqrt{3}}{2} & -1 \end{bmatrix}$	$\begin{bmatrix} -\frac{3}{2} & \frac{\sqrt{3}}{2} & 0 \\ \frac{3}{2} & \frac{-\sqrt{3}}{2} & 0 \\ -\frac{1}{2} & \frac{\sqrt{3}}{2} & 1 \end{bmatrix}$	$\begin{bmatrix} \frac{1}{2} & \frac{\sqrt{3}}{2} & -1 \\ -\frac{3}{2} & \frac{-\sqrt{3}}{2} & 0 \\ \frac{3}{2} & \frac{-\sqrt{3}}{2} & 0 \end{bmatrix}$
6	$\begin{bmatrix} 1 & 0 & 1 \\ \frac{1}{2} & \frac{\sqrt{3}}{2} & -1 \\ 0 & -\sqrt{3} & 0 \end{bmatrix}$	$\begin{bmatrix} \frac{3}{2} & \frac{\sqrt{3}}{2} & 0 \\ -\frac{1}{2} & \frac{-\sqrt{3}}{2} & 1 \\ \frac{1}{2} & \frac{-\sqrt{3}}{2} & -1 \end{bmatrix}$	$\begin{bmatrix} \frac{3}{2} & \frac{\sqrt{3}}{2} & 0 \\ 0 & -\sqrt{3} & 0 \\ -\frac{1}{2} & \frac{\sqrt{3}}{2} & 1 \end{bmatrix}$	$\begin{bmatrix} -1 & 0 & -1 \\ \frac{3}{2} & \frac{\sqrt{3}}{2} & 0 \\ 0 & -\sqrt{3} & 0 \end{bmatrix}$

2.1.4. Simulation Results of a Sensored Speed Control

Figure 6 shows the closed-loop field-oriented speed control structure proposed for the fault-tolerant PMSM drive [25]. The reliability of this topology has been enhanced by adding the fourth leg to control the zero-sequence component using the 3D-SVPWM technique of the current in the case of a loss of one phase. Under normal operating conditions, the controller of the zero-sequence component will maintain neutral voltage V_n to zero. If a fault is introduced to any phase of the motor, then, the controller of the zero-sequence component will change the neutral voltage V_n . The simulation of the PMSM drive system has been carried out using the SABER simulation package in sensed mode pre and post an open-circuit fault.

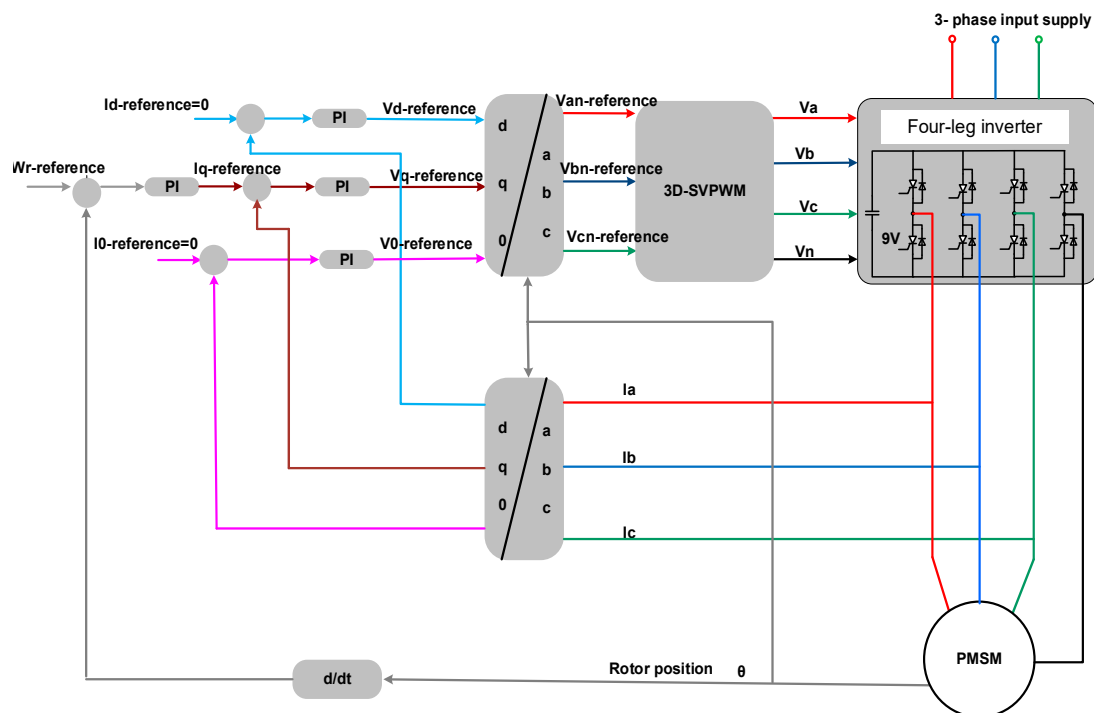


Figure 6. Closed-loop field-oriented speed control topology using 3D-SVPWM for four-leg inverter proposed in [25].

The simulation results in Figure 7 show the feasibility of the system. The motor (see Appendix A) was running at speed equals to 150 rpm at full load and under normal operating conditions. In the time interval (1–2 s), an open-circuit fault is introduced to phase “a”. The motor then returns to normal operating condition in time interval (2–3 s). Following that, in the time interval (3–4 s), an open-circuit fault is introduced to phase “b”. In the time interval (4–5 s), the motor returns to normal operating condition. Finally, in the time interval (5–6 s) an open circuit is introduced to phase “c”. It can be noticed from the results that the speed of the motor is kept constant during this test even under the loss of one phase with minimum ripple in it. Additionally, the currents I_d and I_q are kept constant with minimum ripple. The zero-sequence current changes according to the operating condition. The controllers could maintain the performance of the system post the loss of each phase by increasing the remaining healthy currents by $\sqrt{3}$ as well as phase-shifting them by 30 degrees away from the faulted phase to maintain the rotating magneto motive force (MMF). This action is done automatically by the controller in this work without the need for any extra actions as in [25]. This is related to the using of 3D-SVPWM in which the phase to neutral voltage in each leg can be generated separately unlike the use of 2D-SVPWM.

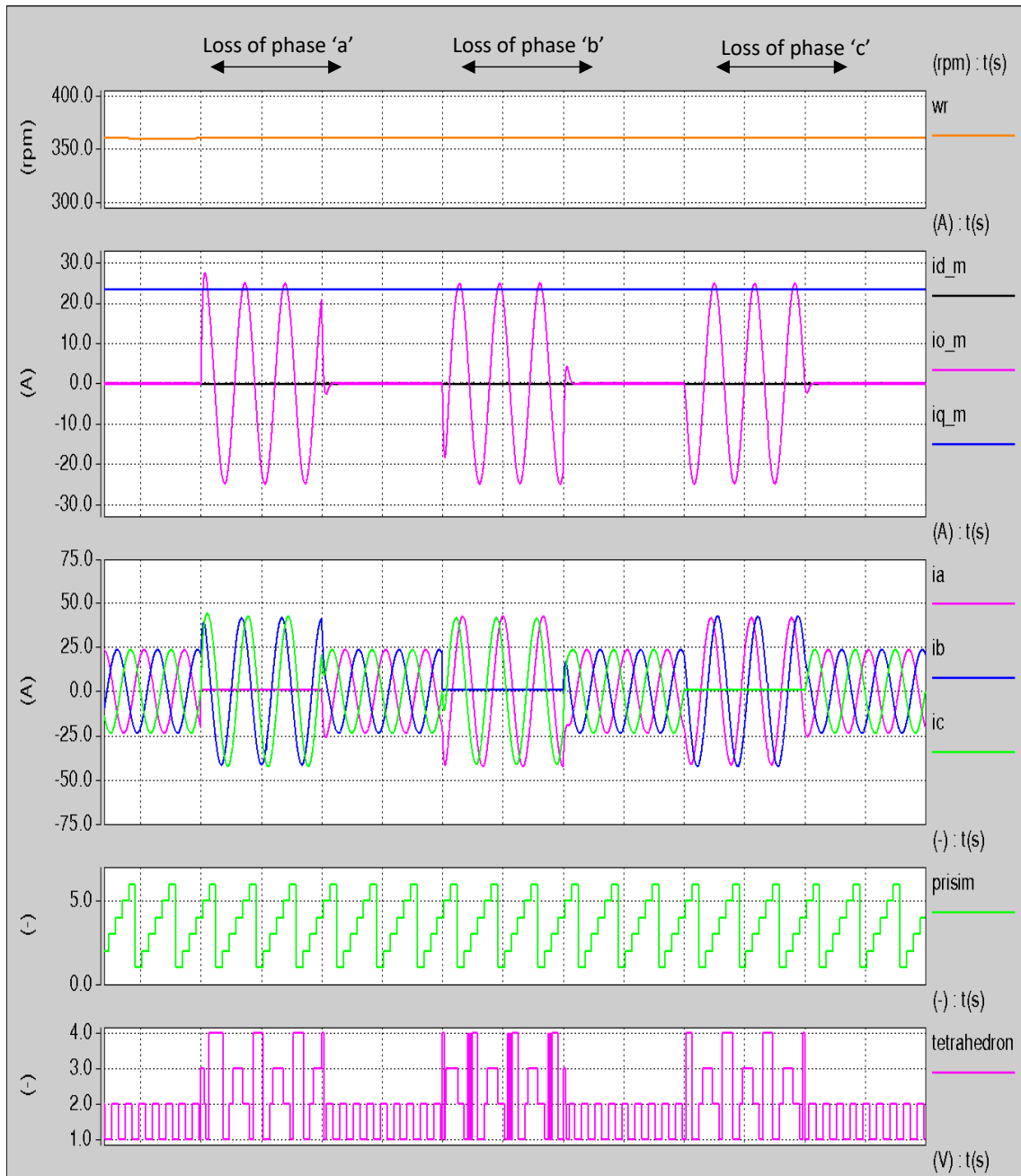


Figure 7. Performance of the fault-tolerant PMSM drive system.

2.2. Saturation Saliency Tracking in PMSM

2.2.1. Healthy Operating Condition

The effects of saturation saliency are included in the model of the PMSM motor as shown in Equation (3). These effects will be reflected in the transient response of the three stator currents of the PMSM motor due to the insulated-gate bipolar transistor (IGBT) switching actions under the normal operating conditions. Hence, by the transient current response of the three currents during each PWM period, it is possible to track the saturation saliency. The algorithm to track the saturation saliency under the normal operating conditions is presented in this section. Figure 8 shows the switching sequence of the fault-tolerant inverter under normal operating condition for the case when the reference voltage exists in prism 5 and tetrahedron 1. The stator circuits when the vectors V0, V1, V2, and V3 are applied are shown in the same figure.

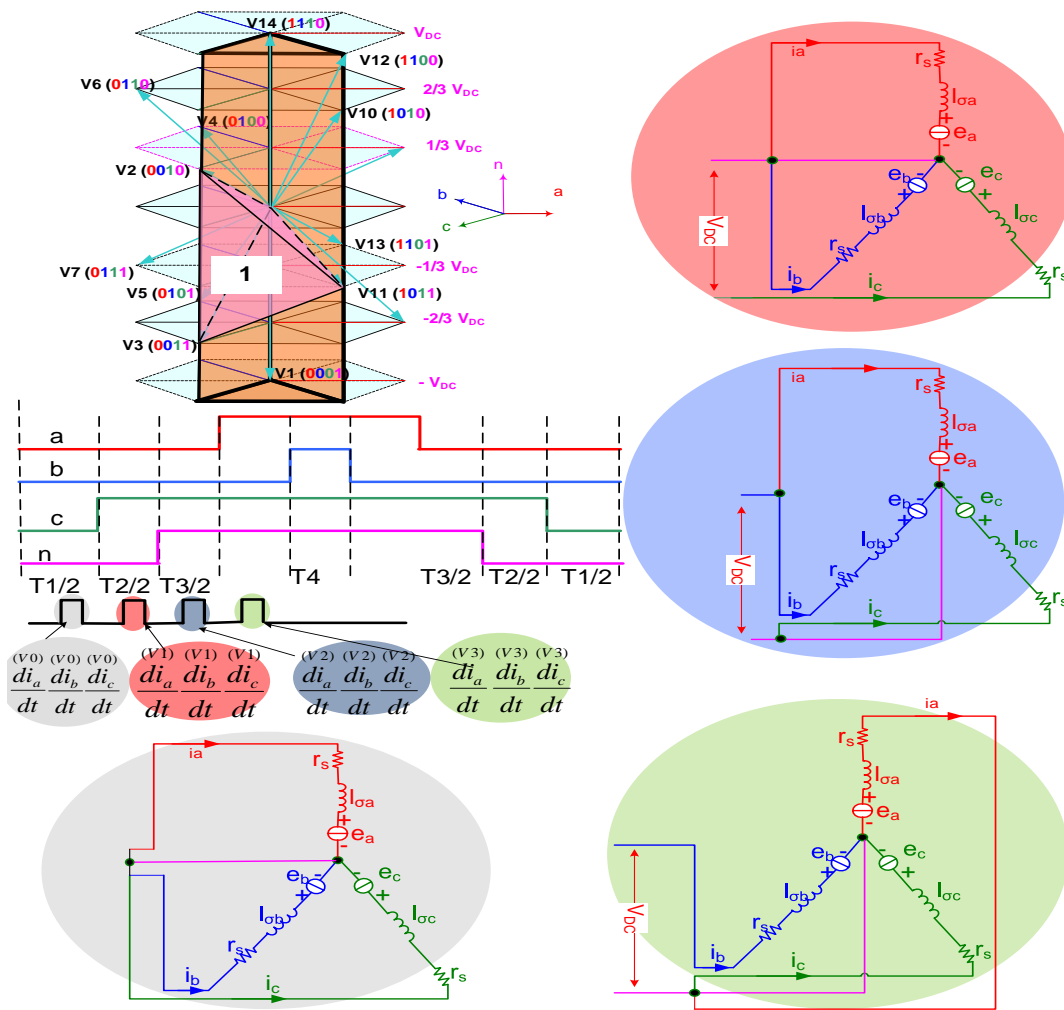


Figure 8. Switching sequence for the case when the reference voltage exists in prism 5 and tetrahedron 1 in 3D SVM and the stator dynamic circuits under application of the voltage vectors V0, V1, V2, and V3 in normal operating conditions.

Using the stator dynamic circuits shown in Figure 8, the following equations hold true.

$$\begin{bmatrix} 0 \\ 0 \\ V_{DC} \end{bmatrix} = r_s * \begin{bmatrix} i_a^{(V1)} - i_a^{(V0)} \\ i_b^{(V1)} - i_b^{(V0)} \\ i_c^{(V1)} - i_c^{(V0)} \end{bmatrix} + \frac{d}{dt} \begin{bmatrix} l_{\sigma a} * (i_a^{(V1)} - i_a^{(V0)}) \\ l_{\sigma b} * (i_b^{(V1)} - i_b^{(V0)}) \\ l_{\sigma c} * (i_c^{(V1)} - i_c^{(V0)}) \end{bmatrix} + \begin{bmatrix} e_a^{(V1)} - e_a^{(V0)} \\ e_b^{(V1)} - e_b^{(V0)} \\ e_c^{(V1)} - e_c^{(V0)} \end{bmatrix} \quad (7)$$

$$\begin{bmatrix} V_{DC} \\ 0 \\ 0 \end{bmatrix} = r_s * \begin{bmatrix} i_a^{(V2)} - i_a^{(V1)} \\ i_b^{(V2)} - i_b^{(V1)} \\ i_c^{(V2)} - i_c^{(V1)} \end{bmatrix} + \frac{d}{dt} \begin{bmatrix} l_{\sigma a} * (i_a^{(V2)} - i_a^{(V1)}) \\ l_{\sigma b} * (i_b^{(V2)} - i_b^{(V1)}) \\ l_{\sigma c} * (i_c^{(V2)} - i_c^{(V1)}) \end{bmatrix} + \begin{bmatrix} e_a^{(V2)} - e_a^{(V1)} \\ e_b^{(V2)} - e_b^{(V1)} \\ e_c^{(V2)} - e_c^{(V1)} \end{bmatrix} \quad (8)$$

$$\begin{bmatrix} 0 \\ V_{DC} \\ 0 \end{bmatrix} = r_s * \begin{bmatrix} i_a^{(V3)} - i_a^{(V2)} \\ i_b^{(V3)} - i_b^{(V2)} \\ i_c^{(V3)} - i_c^{(V2)} \end{bmatrix} + \frac{d}{dt} \begin{bmatrix} l_{\sigma a} * (i_a^{(V3)} - i_a^{(V2)}) \\ l_{\sigma b} * (i_b^{(V3)} - i_b^{(V2)}) \\ l_{\sigma c} * (i_c^{(V3)} - i_c^{(V2)}) \end{bmatrix} + \begin{bmatrix} e_a^{(V3)} - e_a^{(V2)} \\ e_b^{(V3)} - e_b^{(V2)} \\ e_c^{(V3)} - e_c^{(V2)} \end{bmatrix} \quad (9)$$

As the time separation between the vectors V0, V1, V2, and V3 is small (one PWM period), the back EMF can be neglected. Moreover, the voltage drop across the stator resistances is small and can be neglected. Hence, the following equations can be obtained using vector V0, V1, V2, and V3:

$$\begin{bmatrix} V_{DC} \\ 0 \\ 0 \end{bmatrix} = \frac{d}{dt} \begin{bmatrix} l_{\sigma a} * (i_a^{(V1)} - i_a^{(V0)}) \\ l_{\sigma b} * (i_b^{(V1)} - i_b^{(V0)}) \\ l_{\sigma c} * (i_c^{(V1)} - i_c^{(V0)}) \end{bmatrix} \tag{10}$$

$$\begin{bmatrix} 0 \\ V_{DC} \\ 0 \end{bmatrix} = \frac{d}{dt} \begin{bmatrix} l_{\sigma a} * (i_a^{(V2)} - i_a^{(V1)}) \\ l_{\sigma b} * (i_b^{(V2)} - i_b^{(V1)}) \\ l_{\sigma c} * (i_c^{(V2)} - i_c^{(V1)}) \end{bmatrix} \tag{11}$$

$$\begin{bmatrix} 0 \\ 0 \\ V_{DC} \end{bmatrix} = \frac{d}{dt} \begin{bmatrix} l_{\sigma a} * (i_a^{(V3)} - i_a^{(V2)}) \\ l_{\sigma b} * (i_b^{(V3)} - i_b^{(V2)}) \\ l_{\sigma c} * (i_c^{(V3)} - i_c^{(V2)}) \end{bmatrix} \tag{12}$$

Finally the saliency position scalars P_a , P_b , and P_c can be obtained as follows:

$$\begin{bmatrix} P_a \\ P_b \\ P_c \end{bmatrix} = \frac{d}{dt} \begin{bmatrix} (i_a^{(V1)} - i_a^{(V0)}) \\ (i_b^{(V2)} - i_b^{(V1)}) \\ (i_c^{(V3)} - i_c^{(V2)}) \end{bmatrix} \tag{13}$$

By doing the same procedures for other cases Table 5 can be constructed to track the saturation saliency under healthy operating conditions.

Table 5. Selection of the saturation saliency position scalars P_a , P_b , and P_c for a fault-tolerant PMSM drive under normal operating condition.

Prism	Tetrahedron 1	Tetrahedron 2	Tetrahedron 3	Tetrahedron 4
1	$\begin{bmatrix} \frac{d i_a^{V1}}{dt} - \frac{d i_a^{V0}}{dt} \\ \frac{d i_b^{V2}}{dt} - \frac{d i_b^{V1}}{dt} \\ \frac{d i_c^{V4}}{dt} - \frac{d i_c^{V3}}{dt} \end{bmatrix}$	$\begin{bmatrix} \frac{d i_a^{V1}}{dt} - \frac{d i_a^{V0}}{dt} \\ \frac{d i_b^{V2}}{dt} - \frac{d i_b^{V1}}{dt} \\ \frac{d i_c^{V4}}{dt} - \frac{d i_c^{V3}}{dt} \end{bmatrix}$	$\begin{bmatrix} \frac{d i_a^{V1}}{dt} - \frac{d i_a^{V0}}{dt} \\ \frac{d i_b^{V2}}{dt} - \frac{d i_b^{V1}}{dt} \\ \frac{d i_c^{V3}}{dt} - \frac{d i_c^{V2}}{dt} \end{bmatrix}$	$\begin{bmatrix} \frac{d i_a^{V2}}{dt} - \frac{d i_a^{V1}}{dt} \\ \frac{d i_b^{V3}}{dt} - \frac{d i_b^{V2}}{dt} \\ \frac{d i_c^{V4}}{dt} - \frac{d i_c^{V3}}{dt} \end{bmatrix}$
2	$\begin{bmatrix} \frac{d i_a^{V1}}{dt} - \frac{d i_a^{V0}}{dt} \\ \frac{d i_b^{V2}}{dt} - \frac{d i_b^{V1}}{dt} \\ \frac{d i_c^{V4}}{dt} - \frac{d i_c^{V3}}{dt} \end{bmatrix}$	$\begin{bmatrix} \frac{d i_a^{V1}}{dt} - \frac{d i_a^{V0}}{dt} \\ \frac{d i_b^{V2}}{dt} - \frac{d i_b^{V1}}{dt} \\ \frac{d i_c^{V4}}{dt} - \frac{d i_c^{V3}}{dt} \end{bmatrix}$	$\begin{bmatrix} \frac{d i_a^{V1}}{dt} - \frac{d i_a^{V0}}{dt} \\ \frac{d i_b^{V2}}{dt} - \frac{d i_b^{V1}}{dt} \\ \frac{d i_c^{V4}}{dt} - \frac{d i_c^{V3}}{dt} \end{bmatrix}$	$\begin{bmatrix} \frac{d i_a^{V1}}{dt} - \frac{d i_a^{V0}}{dt} \\ \frac{d i_b^{V2}}{dt} - \frac{d i_b^{V1}}{dt} \\ \frac{d i_c^{V4}}{dt} - \frac{d i_c^{V3}}{dt} \end{bmatrix}$
3	$\begin{bmatrix} \frac{d i_a^{V1}}{dt} - \frac{d i_a^{V0}}{dt} \\ \frac{d i_b^{V2}}{dt} - \frac{d i_b^{V1}}{dt} \\ \frac{d i_c^{V4}}{dt} - \frac{d i_c^{V3}}{dt} \end{bmatrix}$	$\begin{bmatrix} \frac{d i_a^{V1}}{dt} - \frac{d i_a^{V0}}{dt} \\ \frac{d i_b^{V2}}{dt} - \frac{d i_b^{V1}}{dt} \\ \frac{d i_c^{V4}}{dt} - \frac{d i_c^{V3}}{dt} \end{bmatrix}$	$\begin{bmatrix} \frac{d i_a^{V1}}{dt} - \frac{d i_a^{V0}}{dt} \\ \frac{d i_b^{V2}}{dt} - \frac{d i_b^{V1}}{dt} \\ \frac{d i_c^{V4}}{dt} - \frac{d i_c^{V3}}{dt} \end{bmatrix}$	$\begin{bmatrix} \frac{d i_a^{V1}}{dt} - \frac{d i_a^{V0}}{dt} \\ \frac{d i_b^{V2}}{dt} - \frac{d i_b^{V1}}{dt} \\ \frac{d i_c^{V4}}{dt} - \frac{d i_c^{V3}}{dt} \end{bmatrix}$
4	$\begin{bmatrix} \frac{d i_a^{V1}}{dt} - \frac{d i_a^{V0}}{dt} \\ \frac{d i_b^{V2}}{dt} - \frac{d i_b^{V1}}{dt} \\ \frac{d i_c^{V4}}{dt} - \frac{d i_c^{V3}}{dt} \end{bmatrix}$	$\begin{bmatrix} \frac{d i_a^{V1}}{dt} - \frac{d i_a^{V0}}{dt} \\ \frac{d i_b^{V2}}{dt} - \frac{d i_b^{V1}}{dt} \\ \frac{d i_c^{V4}}{dt} - \frac{d i_c^{V3}}{dt} \end{bmatrix}$	$\begin{bmatrix} \frac{d i_a^{V1}}{dt} - \frac{d i_a^{V0}}{dt} \\ \frac{d i_b^{V2}}{dt} - \frac{d i_b^{V1}}{dt} \\ \frac{d i_c^{V4}}{dt} - \frac{d i_c^{V3}}{dt} \end{bmatrix}$	$\begin{bmatrix} \frac{d i_a^{V1}}{dt} - \frac{d i_a^{V0}}{dt} \\ \frac{d i_b^{V2}}{dt} - \frac{d i_b^{V1}}{dt} \\ \frac{d i_c^{V4}}{dt} - \frac{d i_c^{V3}}{dt} \end{bmatrix}$
5	$\begin{bmatrix} \frac{d i_a^{V1}}{dt} - \frac{d i_a^{V0}}{dt} \\ \frac{d i_b^{V2}}{dt} - \frac{d i_b^{V1}}{dt} \\ \frac{d i_c^{V4}}{dt} - \frac{d i_c^{V3}}{dt} \end{bmatrix}$	$\begin{bmatrix} \frac{d i_a^{V1}}{dt} - \frac{d i_a^{V0}}{dt} \\ \frac{d i_b^{V2}}{dt} - \frac{d i_b^{V1}}{dt} \\ \frac{d i_c^{V4}}{dt} - \frac{d i_c^{V3}}{dt} \end{bmatrix}$	$\begin{bmatrix} \frac{d i_a^{V1}}{dt} - \frac{d i_a^{V0}}{dt} \\ \frac{d i_b^{V2}}{dt} - \frac{d i_b^{V1}}{dt} \\ \frac{d i_c^{V4}}{dt} - \frac{d i_c^{V3}}{dt} \end{bmatrix}$	$\begin{bmatrix} \frac{d i_a^{V1}}{dt} - \frac{d i_a^{V0}}{dt} \\ \frac{d i_b^{V2}}{dt} - \frac{d i_b^{V1}}{dt} \\ \frac{d i_c^{V4}}{dt} - \frac{d i_c^{V3}}{dt} \end{bmatrix}$
6	$\begin{bmatrix} \frac{d i_a^{V1}}{dt} - \frac{d i_a^{V0}}{dt} \\ \frac{d i_b^{V2}}{dt} - \frac{d i_b^{V1}}{dt} \\ \frac{d i_c^{V4}}{dt} - \frac{d i_c^{V3}}{dt} \end{bmatrix}$	$\begin{bmatrix} \frac{d i_a^{V1}}{dt} - \frac{d i_a^{V0}}{dt} \\ \frac{d i_b^{V2}}{dt} - \frac{d i_b^{V1}}{dt} \\ \frac{d i_c^{V4}}{dt} - \frac{d i_c^{V3}}{dt} \end{bmatrix}$	$\begin{bmatrix} \frac{d i_a^{V1}}{dt} - \frac{d i_a^{V0}}{dt} \\ \frac{d i_b^{V2}}{dt} - \frac{d i_b^{V1}}{dt} \\ \frac{d i_c^{V4}}{dt} - \frac{d i_c^{V3}}{dt} \end{bmatrix}$	$\begin{bmatrix} \frac{d i_a^{V1}}{dt} - \frac{d i_a^{V0}}{dt} \\ \frac{d i_b^{V2}}{dt} - \frac{d i_b^{V1}}{dt} \\ \frac{d i_c^{V4}}{dt} - \frac{d i_c^{V3}}{dt} \end{bmatrix}$

2.2.2. Post an Open-Circuit Fault

The algorithm to track the saliency of the fault-tolerant PMSM drive under the normal operating conditions as given in Table 1 cannot be applied in the case of a loss of one phase. This related to the fact that the dynamic current response of the lost phase is equal zero and hence the position scalar related to the lost phase cannot be constructed. To obtain the algorithm to track the saliency post the loss of one phase, the new stator dynamic circuits should be considered. Figure 9 shows the switching sequence of the fault-tolerant inverter post a loss of phase “c” in the case when the reference voltage exists in prism 5 and tetrahedron 1. The stator circuit when the vectors V0, V1, and V2 are applied is shown in the same figure.

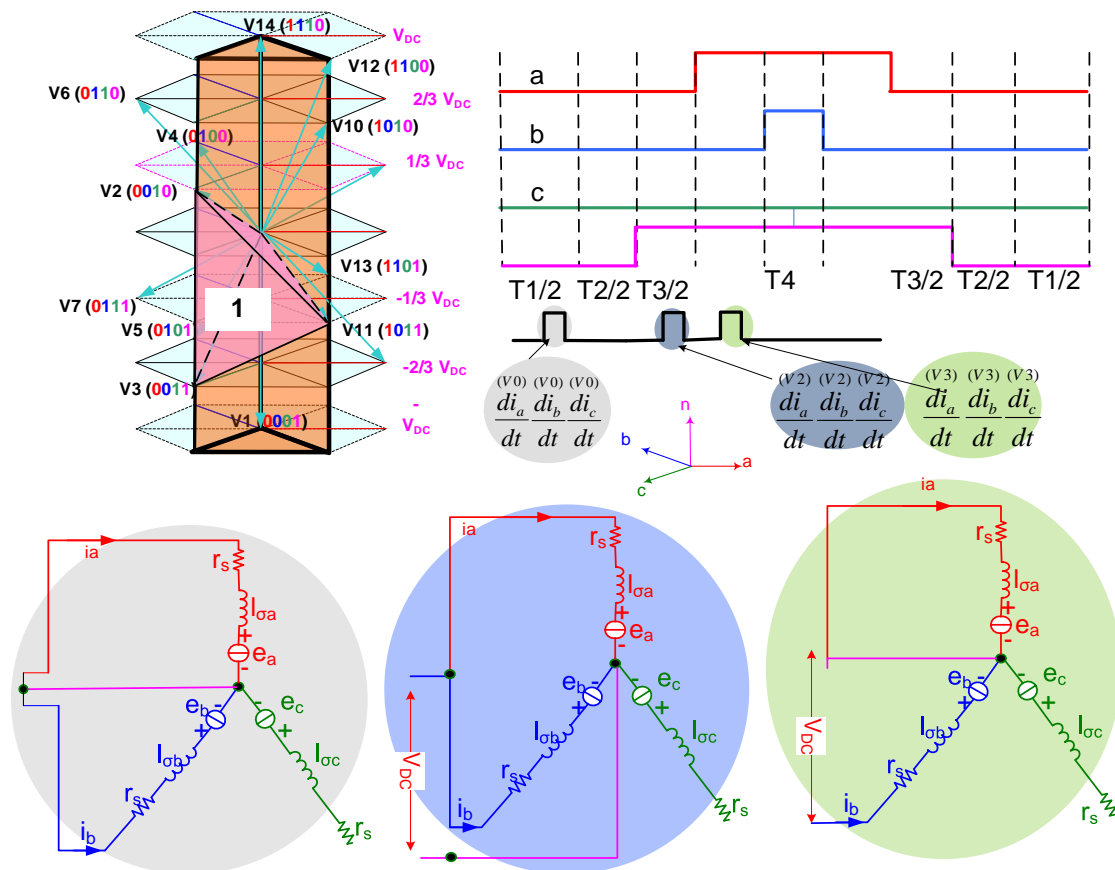


Figure 9. Switching sequence in 3D SVM when the reference voltage exists in prism 5 and tetrahedron 1 and the stator dynamic circuits under application of the voltage vectors V0, V1, and V2 post a loss of phase “c”.

Using the stator dynamic circuits shown in Figure 10, the following equations hold true.

$$\begin{bmatrix} V_{DC} \\ 0 \end{bmatrix} = r_s * \begin{bmatrix} i_a^{(V1)} - i_a^{(V0)} \\ i_b^{(V1)} - i_b^{(V0)} \end{bmatrix} + \frac{d}{dt} \begin{bmatrix} l_{\sigma a} * (i_a^{(V1)} - i_a^{(V0)}) \\ l_{\sigma b} * (i_b^{(V1)} - i_b^{(V0)}) \end{bmatrix} + \begin{bmatrix} e_a^{(V1)} - e_a^{(V0)} \\ e_b^{(V1)} - e_b^{(V0)} \end{bmatrix} \quad (14)$$

$$\begin{bmatrix} 0 \\ V_{DC} \end{bmatrix} = r_s * \begin{bmatrix} i_a^{(V2)} - i_a^{(V1)} \\ i_b^{(V2)} - i_b^{(V1)} \end{bmatrix} + \frac{d}{dt} \begin{bmatrix} l_{\sigma a} * (i_a^{(V2)} - i_a^{(V1)}) \\ l_{\sigma b} * (i_b^{(V2)} - i_b^{(V1)}) \end{bmatrix} + \begin{bmatrix} e_a^{(V2)} - e_a^{(V1)} \\ e_b^{(V2)} - e_b^{(V1)} \end{bmatrix} \quad (15)$$

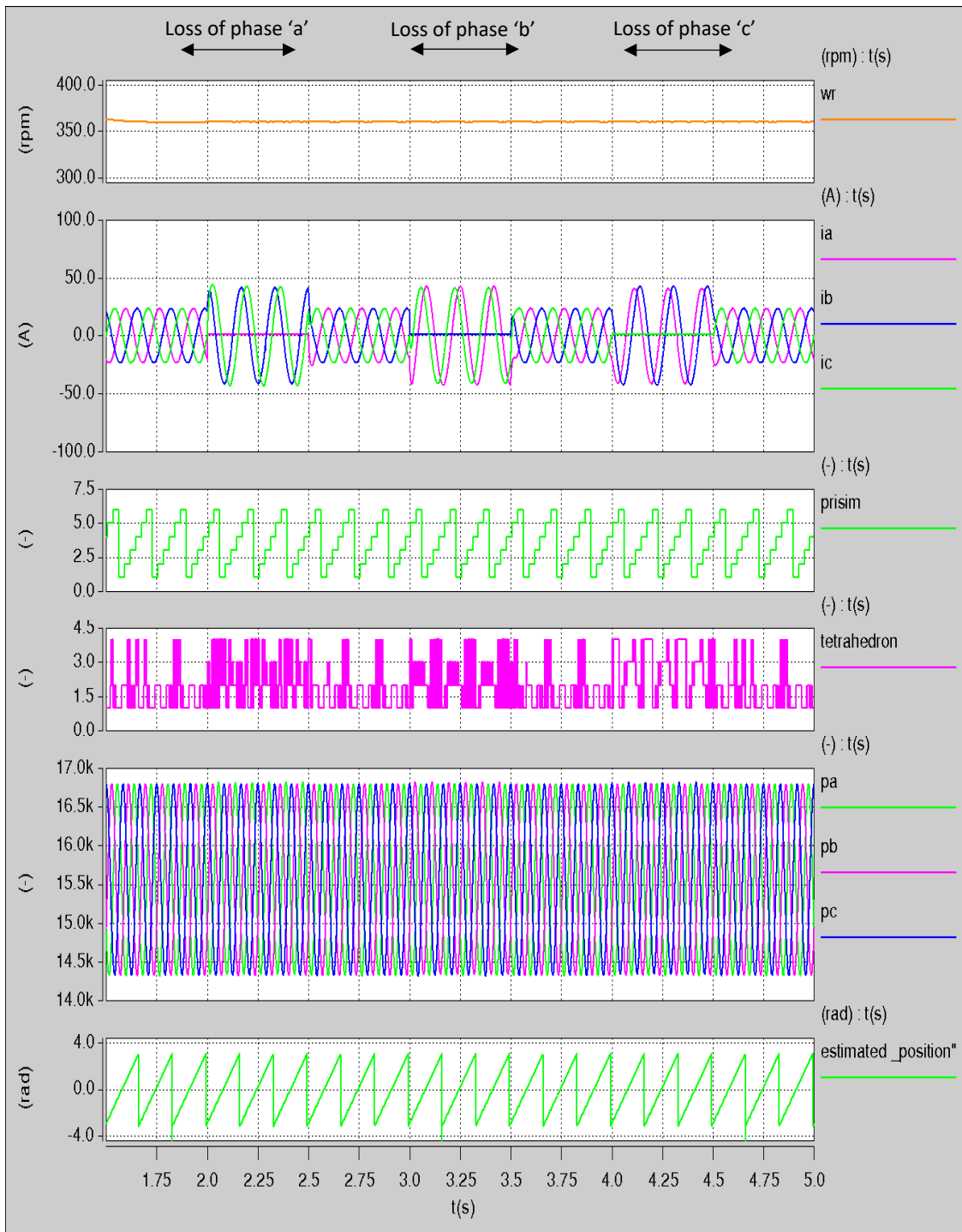


Figure 10. Tracking the saliency in a 4-leg inverter using 3D-SVPWM under normal operating condition and post a loss of one phase.

Using the assumptions mentioned above related to neglecting the back EMF and the voltage drop across the stator resistances, the following equations can be obtained using vectors V_0 , V_1 , and V_2 :

$$\begin{bmatrix} V_{DC} \\ 0 \end{bmatrix} = \frac{d}{dt} \begin{bmatrix} l_{\sigma a} * (i_a^{(V1)} - i_a^{(V0)}) \\ l_{\sigma b} * (i_b^{(V1)} - i_b^{(V0)}) \end{bmatrix} \tag{16}$$

$$\begin{bmatrix} 0 \\ V_{DC} \end{bmatrix} = \frac{d}{dt} \begin{bmatrix} l_{\sigma a} * (i_a^{(V2)} - i_a^{(V1)}) \\ l_{\sigma b} * (i_b^{(V2)} - i_b^{(V1)}) \end{bmatrix} \tag{17}$$

Finally the saliency position scalars P_a and P_b can be obtained as follows:

$$\begin{bmatrix} P_a \\ P_b \end{bmatrix} = \frac{d}{dt} \begin{bmatrix} (i_a^{(V1)} - i_a^{(V0)}) \\ (i_b^{(V2)} - i_b^{(V1)}) \end{bmatrix} \tag{18}$$

P_c can be deduced from P_a and P_b as follows:

$$P_c = -(P_a + P_b) \tag{19}$$

By doing the same procedures for other cases and other phases, Tables 6–8 can be obtained to track the saliency in case of a loss of phase “a”, phase “b”, and phase “c”, respectively.

Table 6. Selection of the saturation saliency position scalars P_a , P_b , and P_c for a fault-tolerant PMSM drive under a loss of phase “a”.

Prism	Tetrahedron 1	Tetrahedron 2	Tetrahedron 3	Tetrahedron 4
1	$\begin{bmatrix} -pb - pc \\ \frac{dib^{V3}}{dt} - \frac{dib^{V2}}{dt} \\ \frac{dic^{V4}}{dt} - \frac{dic^{V3}}{dt} \end{bmatrix}$	$\begin{bmatrix} -pb - pc \\ \frac{dib^{V2}}{dt} - \frac{dib^{V1}}{dt} \\ \frac{dic^{V4}}{dt} - \frac{dic^{V3}}{dt} \end{bmatrix}$	$\begin{bmatrix} -pb - pc \\ \frac{dib^{V2}}{dt} - \frac{dib^{V1}}{dt} \\ \frac{dic^{V3}}{dt} - \frac{dic^{V2}}{dt} \end{bmatrix}$	$\begin{bmatrix} -pb - pc \\ \frac{dib^{V3}}{dt} - \frac{dib^{V2}}{dt} \\ \frac{dic^{V4}}{dt} - \frac{dic^{V3}}{dt} \end{bmatrix}$
2	$\begin{bmatrix} -pb - pc \\ \frac{dib^{V1}}{dt} - \frac{dib^{V0}}{dt} \\ \frac{dic^{V4}}{dt} - \frac{dic^{V3}}{dt} \end{bmatrix}$	$\begin{bmatrix} -pb - pc \\ \frac{dib^{V1}}{dt} - \frac{dib^{V0}}{dt} \\ \frac{dic^{V4}}{dt} - \frac{dic^{V3}}{dt} \end{bmatrix}$	$\begin{bmatrix} -pb - pc \\ \frac{dib^{V1}}{dt} - \frac{dib^{V0}}{dt} \\ \frac{dic^{V3}}{dt} - \frac{dic^{V2}}{dt} \end{bmatrix}$	$\begin{bmatrix} -pb - pc \\ \frac{dib^{V2}}{dt} - \frac{dib^{V1}}{dt} \\ \frac{dic^{V4}}{dt} - \frac{dic^{V3}}{dt} \end{bmatrix}$
3	$\begin{bmatrix} -pb - pc \\ \frac{dib^{V1}}{dt} - \frac{dib^{V0}}{dt} \\ \frac{dic^{V3}}{dt} - \frac{dic^{V2}}{dt} \end{bmatrix}$	$\begin{bmatrix} -pb - pc \\ \frac{dib^{V1}}{dt} - \frac{dib^{V0}}{dt} \\ \frac{dic^{V2}}{dt} - \frac{dic^{V1}}{dt} \end{bmatrix}$	$\begin{bmatrix} -pb - pc \\ \frac{dib^{V1}}{dt} - \frac{dib^{V0}}{dt} \\ \frac{dic^{V2}}{dt} - \frac{dic^{V1}}{dt} \end{bmatrix}$	$\begin{bmatrix} -pb - pc \\ \frac{dib^{V2}}{dt} - \frac{dib^{V1}}{dt} \\ \frac{dic^{V3}}{dt} - \frac{dic^{V2}}{dt} \end{bmatrix}$
4	$\begin{bmatrix} -pb - pc \\ \frac{dib^{V3}}{dt} - \frac{dib^{V2}}{dt} \\ \frac{dic^{V1}}{dt} - \frac{dic^{V0}}{dt} \end{bmatrix}$	$\begin{bmatrix} -pb - pc \\ \frac{dib^{V2}}{dt} - \frac{dib^{V1}}{dt} \\ \frac{dic^{V1}}{dt} - \frac{dic^{V0}}{dt} \end{bmatrix}$	$\begin{bmatrix} -pb - pc \\ \frac{dib^{V2}}{dt} - \frac{dib^{V1}}{dt} \\ \frac{dic^{V1}}{dt} - \frac{dic^{V0}}{dt} \end{bmatrix}$	$\begin{bmatrix} -pb - pc \\ \frac{dib^{V3}}{dt} - \frac{dib^{V2}}{dt} \\ \frac{dic^{V2}}{dt} - \frac{dic^{V1}}{dt} \end{bmatrix}$
5	$\begin{bmatrix} -pb - pc \\ \frac{dib^{V4}}{dt} - \frac{dib^{V3}}{dt} \\ \frac{dic^{V1}}{dt} - \frac{dic^{V0}}{dt} \end{bmatrix}$	$\begin{bmatrix} -pb - pc \\ \frac{dib^{V4}}{dt} - \frac{dib^{V3}}{dt} \\ \frac{dic^{V1}}{dt} - \frac{dic^{V0}}{dt} \end{bmatrix}$	$\begin{bmatrix} -pb - pc \\ \frac{dib^{V3}}{dt} - \frac{dib^{V2}}{dt} \\ \frac{dic^{V1}}{dt} - \frac{dic^{V0}}{dt} \end{bmatrix}$	$\begin{bmatrix} -pb - pc \\ \frac{dib^{V4}}{dt} - \frac{dib^{V3}}{dt} \\ \frac{dic^{V2}}{dt} - \frac{dic^{V1}}{dt} \end{bmatrix}$
6	$\begin{bmatrix} -pb - pc \\ \frac{dib^{V4}}{dt} - \frac{dib^{V3}}{dt} \\ \frac{dic^{V3}}{dt} - \frac{dic^{V2}}{dt} \end{bmatrix}$	$\begin{bmatrix} -pb - pc \\ \frac{dib^{V4}}{dt} - \frac{dib^{V3}}{dt} \\ \frac{dic^{V2}}{dt} - \frac{dic^{V1}}{dt} \end{bmatrix}$	$\begin{bmatrix} -pb - pc \\ \frac{dib^{V3}}{dt} - \frac{dib^{V2}}{dt} \\ \frac{dic^{V2}}{dt} - \frac{dic^{V1}}{dt} \end{bmatrix}$	$\begin{bmatrix} -pb - pc \\ \frac{dib^{V4}}{dt} - \frac{dib^{V3}}{dt} \\ \frac{dic^{V3}}{dt} - \frac{dic^{V2}}{dt} \end{bmatrix}$

2.2.3. Closed Loop Field Oriented Fully Sensorless Speed Control of the PMSM Drive Post a Loss of One Phase

The closed-loop field-oriented encoderless speed control for a PM machine has been simulated with SABER. The saturation saliency position signals $P_{a,b,c}$ are used in a mechanical observer [27] to obtain a cleaned quantity for the rotor speed $\hat{\omega}$ and position $\hat{\theta}$. Moreover, to make the simulation more realistic, a minimum pulse width of 10 μ s is introduced to the di/dt measurements, similar to the experimental results of [12]. Then, the estimated speed $\hat{\omega}$ and position $\hat{\theta}$ are used to obtain a closed-loop field-oriented fully encoderless speed control as shown in Figure 11.

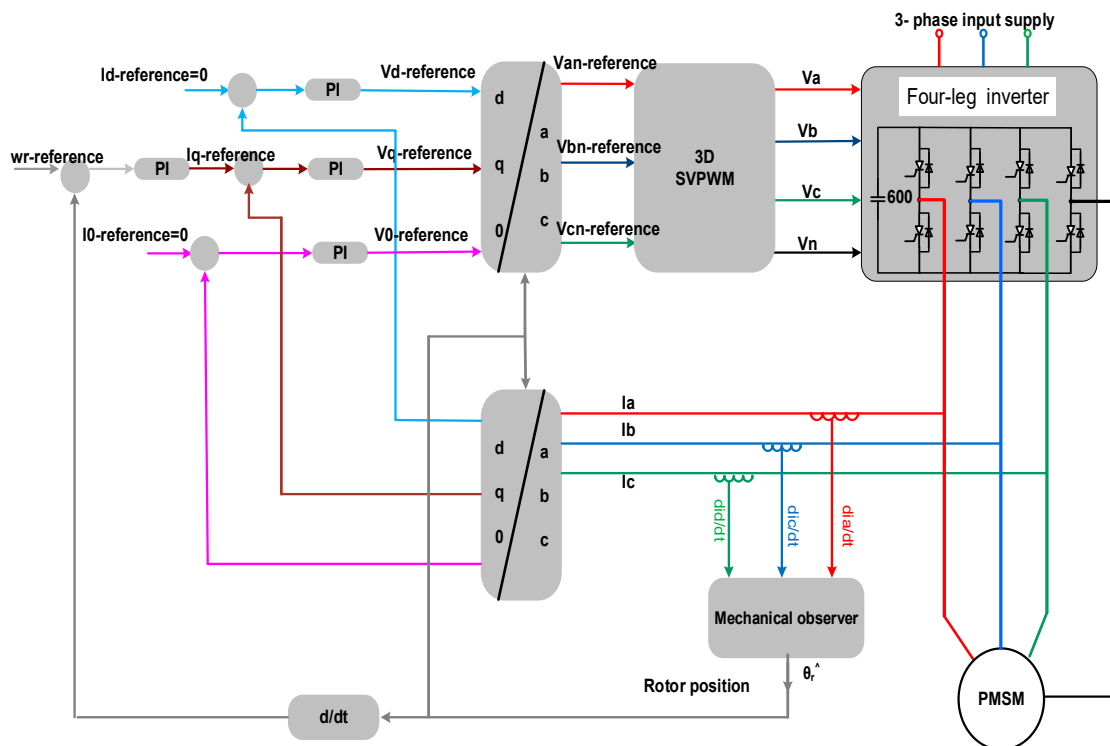


Figure 11. Closed-loop field-oriented encoderless speed control topology using 3D-SVPWM under a loss of one phase.

Figure 12 demonstrates low-speed results of a closed-loop field-oriented encoderless speed control under normal operating conditions and post a loss of one phase using the algorithms proposed in this paper. The motor was running in healthy mode at speed of a 30 rpm. At $t = 2$ s, phase “a” of the motor was lost. Then at $t = 2.5$ s, the speed reference is set to zero. Between $t = 3$ s and $t = 4$ s, the motor returned to normal operating condition. At $t = 4$ s, phase “b” of the motor was lost. After that, at $t = 4.5$ s, the speed reference is set to -30 rpm. Between time $t = 5$ s and $t = 6$ s, the motor returned to normal operating condition. Finally, at time $t = 6$ s phase “c” of the motor was lost. Figure 12 shows that the motor responded to the speed commands with a good transient and steady-state response under pre and post the loss of one phase.

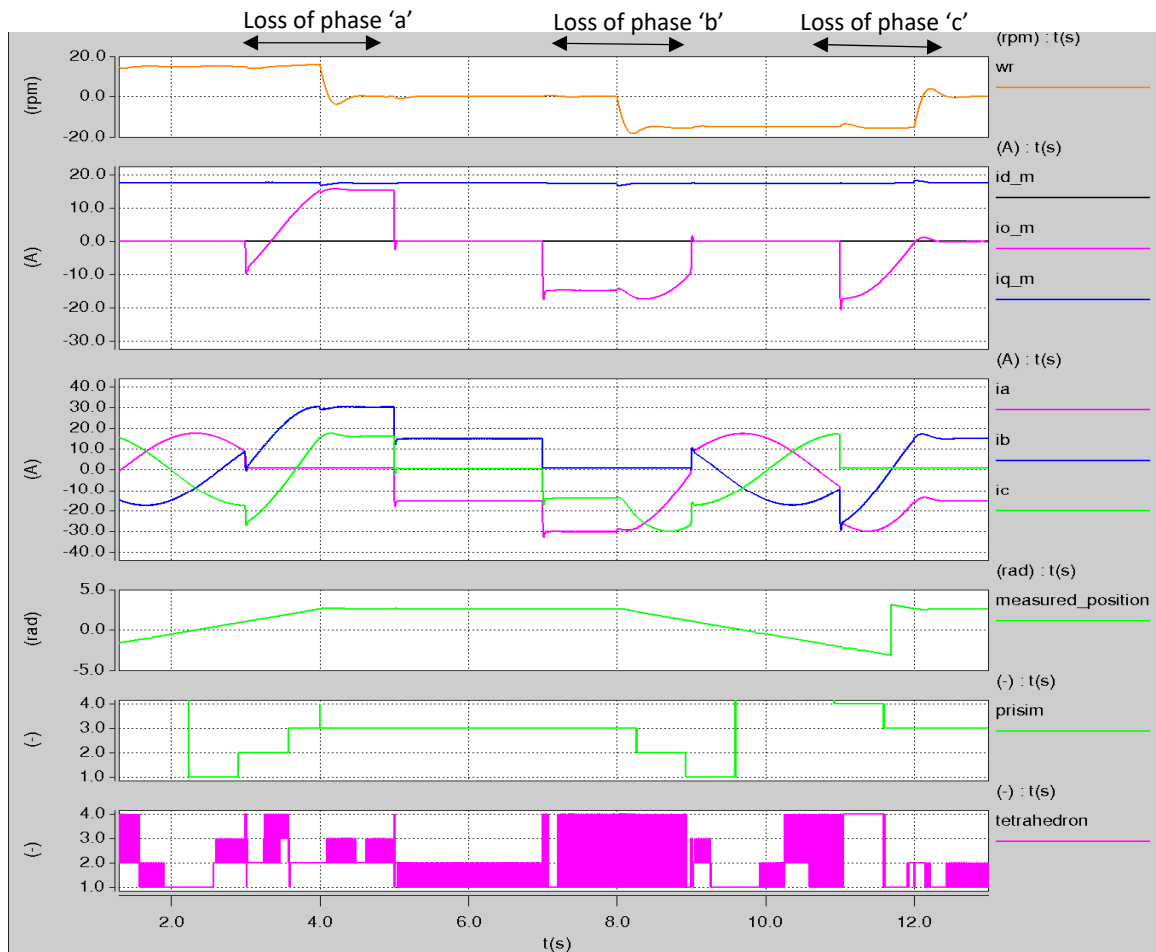


Figure 12. Fully encoderless speed steps between -30 and 30 rpm under different operating conditions.

Figure 13 demonstrates a high-speed result of a closed-loop field-oriented encoderless speed control under normal operating conditions and post a loss of one phase. The figure shows the effectiveness of the system in responding to the high-speed commands (from 500 to -500 rpm and back to 500 rpm) under normal condition as well as when one phase of the motor was lost.

Figure 14 demonstrates the stability of the fully encoderless system when a load disturbance is applied at low speed (150 rpm) pre and post the loss of one phase. The results show that the system maintains the speed in all the cases.

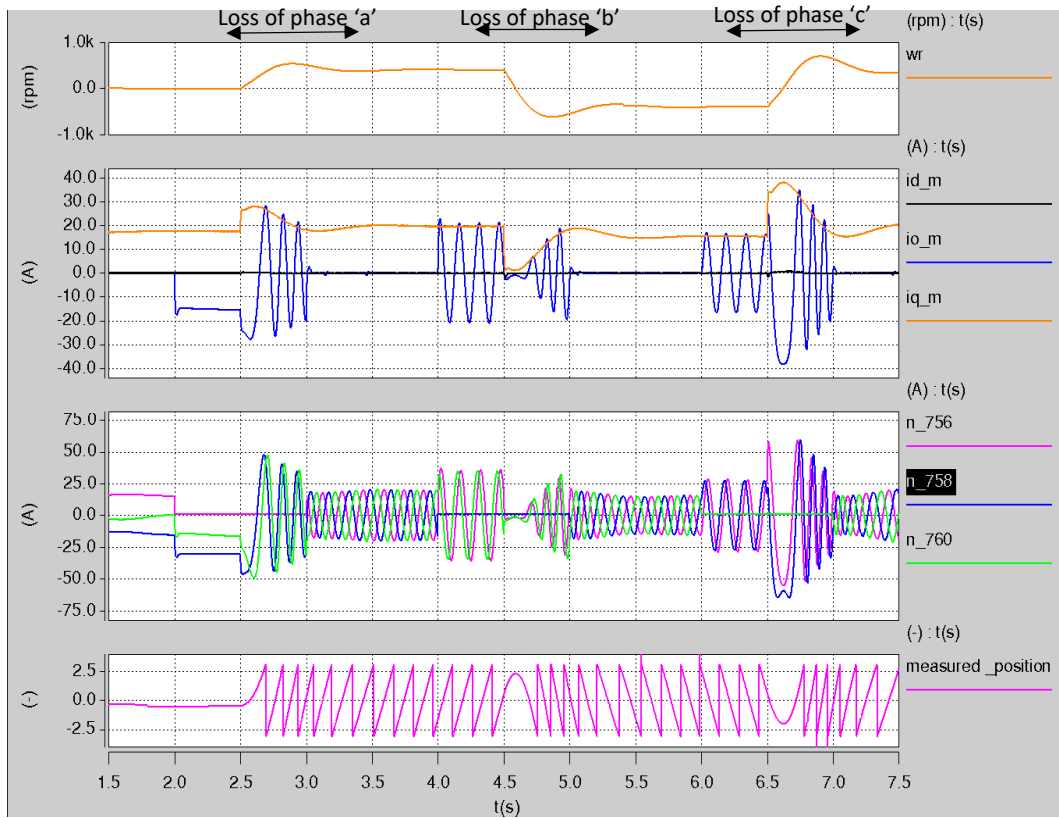


Figure 13. Fully encoderless speed steps between 500 and -500 rpm under different operating conditions.

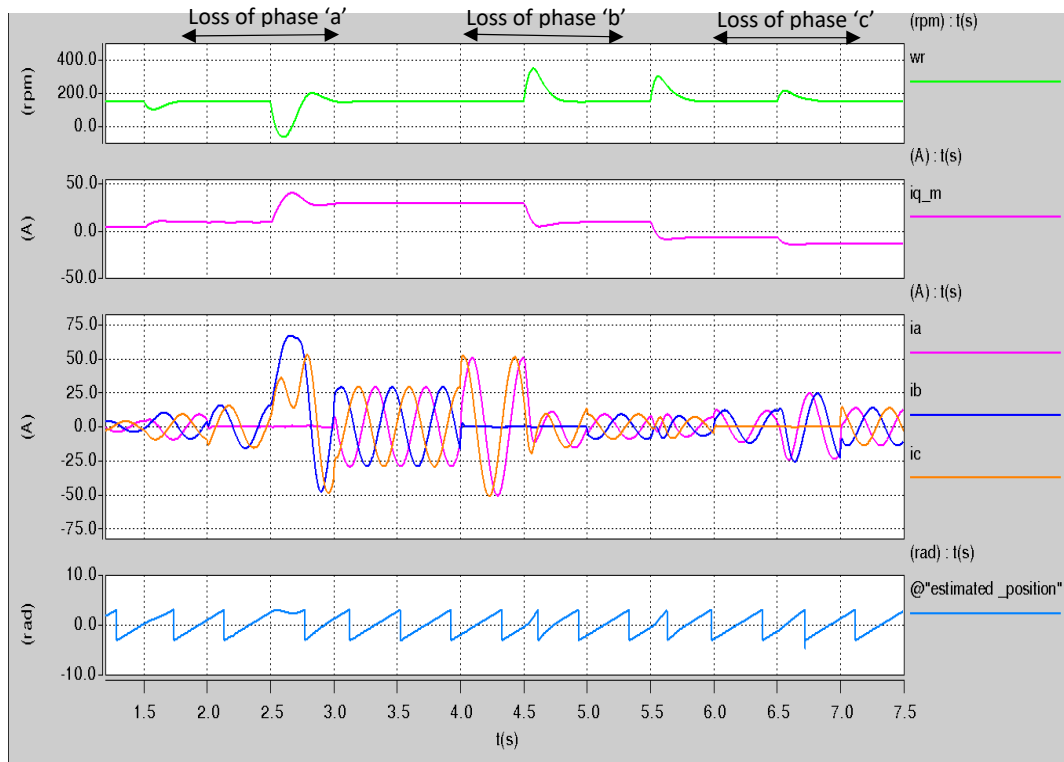


Figure 14. Fully encoderless speed control under different load conditions.

3. Conclusions

This paper has presented an encoderless speed control of a PMSM synchronous motor based on a 3D-SVPWM technique. The PMSM motor was fed from a fault-tolerant inverter that consists of four legs. The saliency position was obtained under the normal conditions as well as when one phase of the motor was lost as follows: firstly the dynamic current responses of the healthy motor line currents due to the insulated-gate bipolar transistor (IGBT) switching actions were obtained. Then, according to the operating condition (normal or a loss of one phase), the saliency position signals were constructed from the dynamic current responses. The new technique can be used to track both the saturation saliency in PM motors ($2 \times f_e$) and the rotor slotting saliency in IMs ($14 \times f_r$). The results have shown the effectiveness of the new method in increasing the safety measures in critical systems that need continuous operation.

Author Contributions: K.S. and M.S. conceived and designed the experiments; K.S. performed the experiments; K.S. analyzed the data; K.S. contributed reagents/materials/analysis tools; K.S. and M.S. wrote the paper. All authors have read and agreed to the published version of the manuscript.

Funding: This research received no external funding.

Conflicts of Interest: The authors declare no conflicts of interest.

Appendix A

The motor parameters are: rated speed = 2000 rpm, rated torque = 10.3 Nm, rated power = 2.15 kW, $K_t = 2 \text{ Nm/A}$, $K_e = 147.0 \text{ Vrms/krpm}$, inertia = 20.5 kgcm², $R(\text{ph-ph}) = 4 \text{ } \Omega$, $L(\text{ph-ph}) = 29.8 \text{ mH}$.

References

1. Vafaie, M.H.; Dehkordi, B.M.; Moallem, P.; Kiyomarsi, A. Improving the steady-state and transient-state performances of PMSM through an advanced deadbeat direct torque and flux control system. *IEEE Trans. Power Electron.* **2017**, *32*, 2964–2975. [[CrossRef](#)]
2. Shinohara, A.; Inoue, Y.; Morimoto, S.; Sanada, M. Direct calculation method of reference flux linkage for maximum torque per ampere control in DTC-based IPMSM drives. *IEEE Trans. Power Electron.* **2017**, *32*, 2114–2122. [[CrossRef](#)]
3. Wang, Y.; Xu, Y.; Zou, J. Sliding mode sensorless control of PMSM with inverter nonlinearity compensation. *IEEE Trans. Power Electron.* **2019**, *34*, 1450–1460. [[CrossRef](#)]
4. Bao, D.; Pan, Y.; Wang, X.; Li, K. Adaptive synchronous-frequency tracking-mode observer for the sensorless control of a surface PMSM. *IEEE Trans. Ind. Electron.* **2018**, *54*, 6460–6471. [[CrossRef](#)]
5. Xu, W.; Jiang, Y.; Mu, C.; Blaabjerg, F. Improved nonlinear flux observer-based second-order SOIFO for PMSM sensorless control. *IEEE Trans. Power Electron.* **2019**, *34*, 565–579. [[CrossRef](#)]
6. Wang, G.; Yang, B.; Zhang, G.; Zhang, X.; Xu, D. Comparative investigation of pseudorandom high-frequency signal injection schemes for sensorless IPMSM drives. *IEEE Trans. Power Electron.* **2017**, *32*, 2123–2132. [[CrossRef](#)]
7. Chen, Z.; Wang, F.; Luo, G.; Zhang, Z.; Kennel, R. Secondary saliency tracking-based sensorless control for concentrated winding SPMSM. *IEEE Trans. Ind. Informat.* **2016**, *12*, 201–210. [[CrossRef](#)]
8. Ronggang, N.; Kaiyuan, L.; Blaabjerg, F.; Dianguo, X. A comparative study on pulse sinusoidal high frequency voltage injection and INFORM methods for PMSM position sensorless control. In Proceedings of the Conference of the IEEE Industrial Electronics Society, Florence, Italy, 23–26 October 2016; pp. 2600–2605.
9. Linke, M.; Kennel, R.; Holtz, J. Sensorless Speed and Position Control of Synchronous Machines using Alternating Carrier Injection. In Proceedings of the IEEE International Electric Machines and Drives Conference IEMDC03, Madison, WI, USA, 1–4 June 2003; Volume 2, pp. 1211–1217.
10. Schroedl, M. Sensorless Control of AC Machines at Low Speed and Standstill Based on the INFORM Method. In Proceedings of the IEEE IAS Annual Meeting, San Diego, CA, USA, 6–10 October 1996; Volume 4, pp. 270–277.
11. Holtz, J.; Juliet, J. Sensorless Acquisition of the Rotor Position Angle of Induction Motors with Arbitrary Stator Windings. In Proceedings of the IAS Annual Meeting, Detroit, MI, USA, 11–15 October 2020; pp. 1675–1682.

12. Qiang, G.; Asher, G.M.; Sumner, M.; Makys, P. Position Estimation of AC Machines at all Frequencies Using Only Space Vector PWM based Excitation. In Proceedings of the 3rd IET International Conference, Seattle, WA, USA, 3–7 October 2004; pp. 61–70.
13. Zhang, W.; Xu, D.; Li, X.; Xie, R.; Li, H.; Dong, D.; Sun, C.; Chen, M. Seamless Transfer Control Strategy for Fuel Cell Uninterruptible Power Supply System. *IEEE Trans. Power Electron.* **2013**, *28*, 717–729. [[CrossRef](#)]
14. Welchko, B.A.; Lipo, T.A.; Jahns, T.M.; Schulz, S.E. Fault tolerant three-phase AC motor drive topologies: A comparison of features, cost, and limitations. *IEEE Trans. Power Electron.* **2004**, *19*, 1108–1116. [[CrossRef](#)]
15. Haimin, T.; Duarte, J.L.; Hendrix, M.A.M. Line-interactive UPS using a fuel cell as the primary source. *IEEE Trans. Ind. Electron.* **2008**, *55*, 3012–3021. [[CrossRef](#)]
16. Zhang, W.; Xu, D.; Enjeti, P.N.; Li, H.; Hawke, J.T.; Krishnamoorthy, H.S. Survey on Fault-Tolerant Techniques for Power Electronic Converters. *IEEE Trans. Power Electron.* **2014**, *29*, 6319–6331. [[CrossRef](#)]
17. Lezana, P.; Pou, J.; Meynard, T.A.; Rodriguez, J.; Ceballos, S.; Richardeau, F. Survey on Fault Operation on Multilevel Inverters. *IEEE Trans. Ind. Electron.* **2010**, *57*, 2207–2218. [[CrossRef](#)]
18. Campos-Delgado, D.U.; Espinoza-Trejo, D.R.; Palacios, E. Faulttolerant control in variable speed drives: A survey. *IET Electr. Power Appl.* **2008**, *2*, 121–134. [[CrossRef](#)]
19. Rodriguez, M.A.; Claudio, A.; Theilliol, D.; Vela, L.G.; Hernandez, L. A strategy to replace the damaged element for fault-tolerant induction motor drive. In Proceedings of the 2008 5th International Conference on Electrical Engineering, Computing Science and Automatic Control, Mexico City, Mexico, 12–14 November 2008; pp. 51–55.
20. Fu, J.; Lipo, T.A. Disturbance free operation of a multiphase current regulated motor drive with an opened phase. *IEEE Trans. Ind. Appl.* **1994**, *30*, 1267–1274.
21. Mohammadpour, A.; Sadeghi, S.; Parsa, L. A Generalized FaultTolerant Control Strategy for Five-Phase PM Motor Drives Considering Star, Pentagon, and Pentacle Connections of Stator Windings. *IEEE Trans. Ind. Electron.* **2014**, *61*, 63–75. [[CrossRef](#)]
22. Yi, Z.; Hongge, S.; Bin, X. Optimization of neutral shift in cell-fault treatment for cascaded H-bridge inverter. In Proceedings of the ICEMS, Wuhan, China, 17–20 October 2008; pp. 1683–1685.
23. Lezana, P.; Ortiz, G. Extended operation of cascade multicell converters under fault condition. *IEEE Trans. Ind. Electron.* **2009**, *56*, 2697–2703. [[CrossRef](#)]
24. Correa, P.; Pacas, M.; Rodriguez, J. Modulation Strategies for FaultTolerant Operation of H-Bridge Multilevel Inverters. In Proceedings of the 2006 IEEE International Symposium on Industrial Electronics, Montreal, QC, Canada, 9–13 July 2006; Volume 2, pp. 1589–1594.
25. Saleh, K.; Sumner, M. Modeling and simulation of sensorless control of four-leg inverter PMSM drives in the case of a single-phase open circuit fault. *Turk. J. Electr. Eng. Comput. Sci.* **2016**, *24*, 3807–3820. [[CrossRef](#)]
26. Zhang, R.; Prasad, V.H.; Boroyevich, D.; Lee, F.C. Three-dimensional space vector modulation for four-leg voltage-source converters. *IEEE Trans. Power Electron.* **2002**, *17*, 314–326. [[CrossRef](#)]
27. Lorenz, R.D.; van Patten, K.W. High-Resolution Velocity Estimation for All-Digital, ac Servo Drives. *IEEE Trans. Ind. Appl.* **1991**, *27*, 701–705. [[CrossRef](#)]

